Supporting Information

Estimating Ground-Level $PM_{2.5}$ in China Using Satellite Remote Sensing

Zongwei Ma [a, b], Xuefei Hu[b], Lei Huang [a], Jun Bi [a,*], Yang Liu [b,*]

[a] State Key Laboratory of Pollution Control and Resource Reuse, School of the Environment, Nanjing University, Xianlin Campus, Box 624, 163 Xianlin Avenue, Nanjing 210023, China

[b] Department of Environmental Health, Rollins School of Public Health, Emory University, 1518 Clifton Road NE, Atlanta, Georgia 30322, United States

[*] Corresponding authors.

Tel.: +1-404-727-2131; Fax: +1-404-727-8744; E-mail: yang.liu@emory.edu (Y. Liu).

Tel.: +86-25-89680566; Fax: +86-25-89680586; E-mail: jbi@nju.edu.cn (J. Bi).

Number of Pages: 20

Number of Figures: 8

Number of Tables: 3

Text S1: AOD data calibration

To improve the data coverage of satellite AOD, we fused Terra MODIS, Aqua MODIS, and MISR AOD retrievals. First, we calibrated Terra MODIS, Aqua MODIS, and MISR AOD data against AERONET AOD data separately. We compared the overall relationships of MODIS Terra AOD~AERONET AOD, MODIS Aqua AOD~AERONET AOD, and MISR AOD~AERONET AOD with previous studies. The regression slope and intercept by satellite AOD against AERONET AOD are as follows: MODIS Terra AOD, 1.00 and 0.05, respectively (N=4,928, R^2=0.83); MODIS Aqua, 1.04 and 0.07, respectively (N=3,693, R^2=0.80); and MISR AOD, 0.58 and 0.07, respectively (N=1,124, R^2=0.81). These results are very similar to previous studies[1-3]. The seasonal, linear regression relationships for Terra, Aqua, and MISR AOD calibrations are shown in Table S1. The relationships vary by season and AOD dataset. Then, Terra MODIS, Aqua MODIS, and MISR data were calibrated using the established relationships in Table S1, respectively. We also considered regional satellite AOD and AERONET AOD relationships. However, the AERONET AOD data are scarce in some areas (e.g., bright desert areas), making it difficult to establish a robust relationship between the two types of AOD. Thus, we use a single relation across China instead.

Table S1 Linear regression results for MODIS and MISR AOD Calibration

Seasons	$\hat{\tau}_{\mathrm{AERO}} = \beta_1 * \tau_{\mathrm{Terra}} + \alpha_1$			$\hat{\tau}_{\mathrm{AERO}} = \beta_1 * \tau_{\mathrm{Aqua}} + \alpha_1$			$\hat{\tau}_{\mathrm{AERO}} = \beta_1 * \tau_{\mathrm{MISR}} + \alpha_1$		
	α_1	β_1	R^2	α_2	β_2	R^2	α_2	β_2	R^2
Winter	0.04	0.88	0.76	0.05	0.80	0.72	-0.03	1.50	0.78
Spring	0.03	0.79	0.82	0.04	0.74	0.77	-0.07	1.45	0.77
Summer	0.02	0.81	0.81	0.00	0.77	0.80	-0.03	1.34	0.87
Autumn	0.00	0.96	0.87	0.02	0.86	0.83	-0.02	1.46	0.83

$\hat{\tau}$- Aerosol Optical Depth

Text S2: AOD data fusion

For the AOD data fusion, we first averaged the calibrated Terra MODIS, Aqua MODIS, and MISR AOD over the 50 km grid cells. Due to the different satellite overpass times, we first applied simple linear regression between Terra MODIS and Aqua MODIS AOD data in those 50km grid cells where both these two kinds of MODIS products are present for each day. We first considered the local- or regional-scale relationships between Aqua and Terra MODIS AOD, which are more reasonable. However, due to variation in cloud coverage or bright surfaces such as snow and desert, spatial AOD coverage differs on different days. Uncertainty in the data fusion may be elevated in some regions where there are too few data points to build a robust relationship between Aqua and Terra. Thus we assumed that the relationship between Aqua and Terra was the same across the study area on each day. The results show that the number of daily matched Terra and Aqua AOD grid cells ranges from 35 to 1,883, with mean, standard deviation, and median values of 662, 363, and 624, respectively. The daily Terra-Aqua MODIS AOD regression R^2 values range from 0.49 to 0.95, with the mean, standard deviation, and median values of 0.81, 0.09, and 0.83, respectively. The results show that the Terra MODIS AOD is highly correlated with the Aqua MODIS AOD for each day, and it is feasible to predict the missing Terra MODIS AOD values using the Aqua MODIS AOD values. The daily regression coefficients were applied to each grid cell to predict the missing Terra MODIS AOD using the available Aqua MODIS AOD. For those grid cells where both MODIS AOD values are missing, we used MISR AOD data instead.

The coverages of fused AOD, MODIS AOD, and MISR AOD are shown in Figure S1, Figure S2, and Figure S3, respectively. MODIS collection 5.1 aerosol products over land are retrieved by Dark Target

(DT) algorithms [4], by which AOD values cannot be retrieved over bright surfaces, such as desert and snow. Thus the MODIS AOD coverage over Xinjiang, Tibet, and Qinghai during the winter and spring are relatively low, and may even approach zero. Unlike MODIS, MISR aerosol products are retrieved by Empirical Orthogonal Functions EOFs) [5], which has the capacity to retrieve AOD values over bright surfaces. Comparing Figure S1 with Figure S2 and Figure S3, most of the AOD retrievals in Tibet, Xinjiang, and Qinghai are from MISR, especially in the winter and spring.

MODIS Collection 5.1 aerosol products contain the AOD data retrieved by the Deep Blue (DB) algorithm. The DB algorithm was developed for retrieving aerosol properties over bright-reflecting surfaces [6]. However, previous validation of DB AOD in China reveals a serious underestimation over desert areas [7]. Besides, at the time of this study, DB product was only available for Aqua MODIS for the years 2008 through 2013. Due to the different satellite overpass times, the DB product cannot be merged with Terra MODIS AOD, and MISR AOD, and thus was not included in this study. The next version of MODIS aerosol products (Collection 6, C6) has been developed [8]. The MODIS C6 products include the second-generation DB algorithm [9], which is expected to improve the accuracy of DB AOD. The MODIS C6 products have a combined product that merges DT and DB AOD data to improve the data coverage [8]. At the time of this study, MODIS C6 data were only available in Aqua MODIS products for the years of 2002 through 2008.

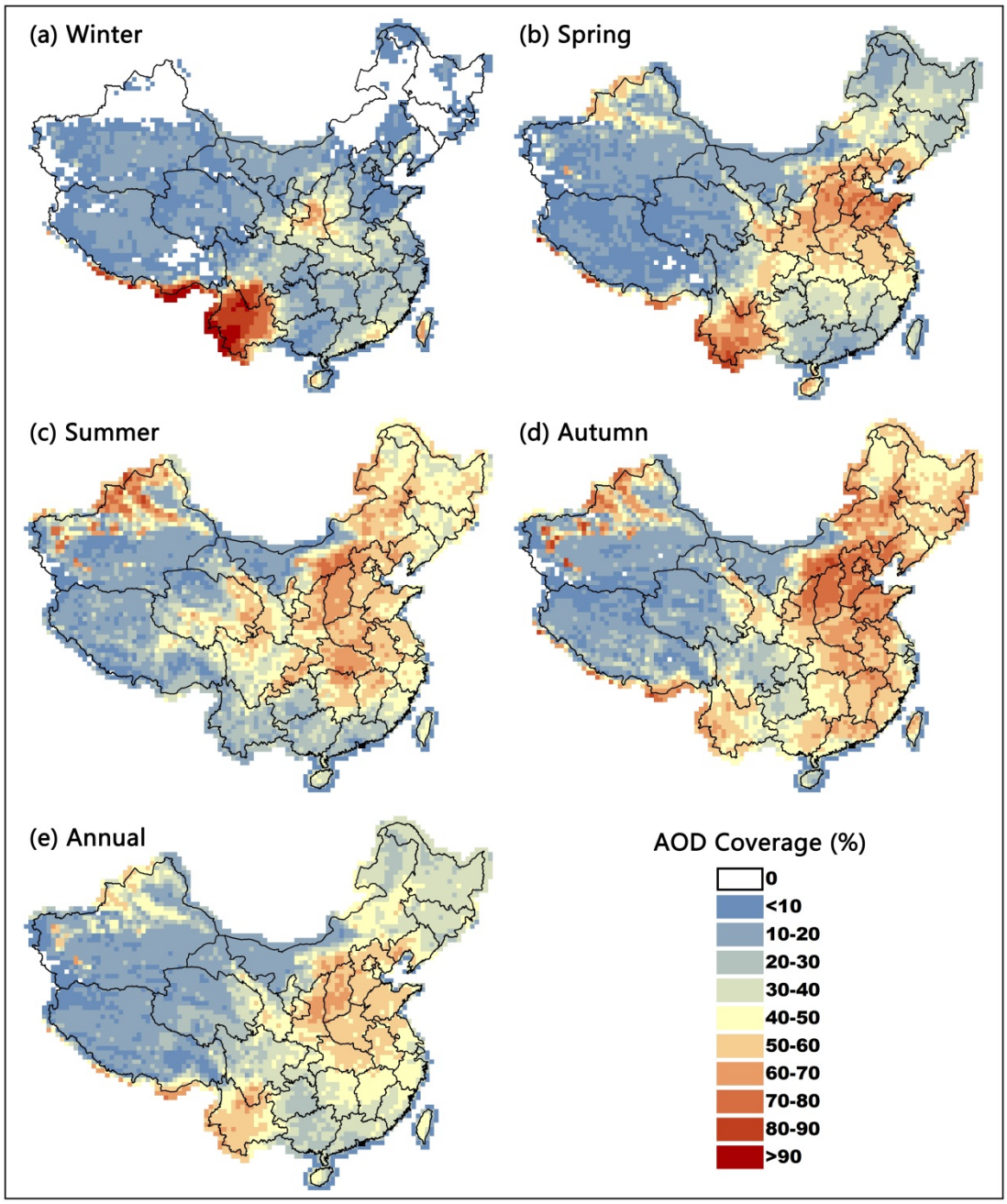

Figure S1. The spatial distribution of percent coverage of fused AOD. The percent coverage denotes the percentage of the AOD available days of each season or the whole year for each grid cell.

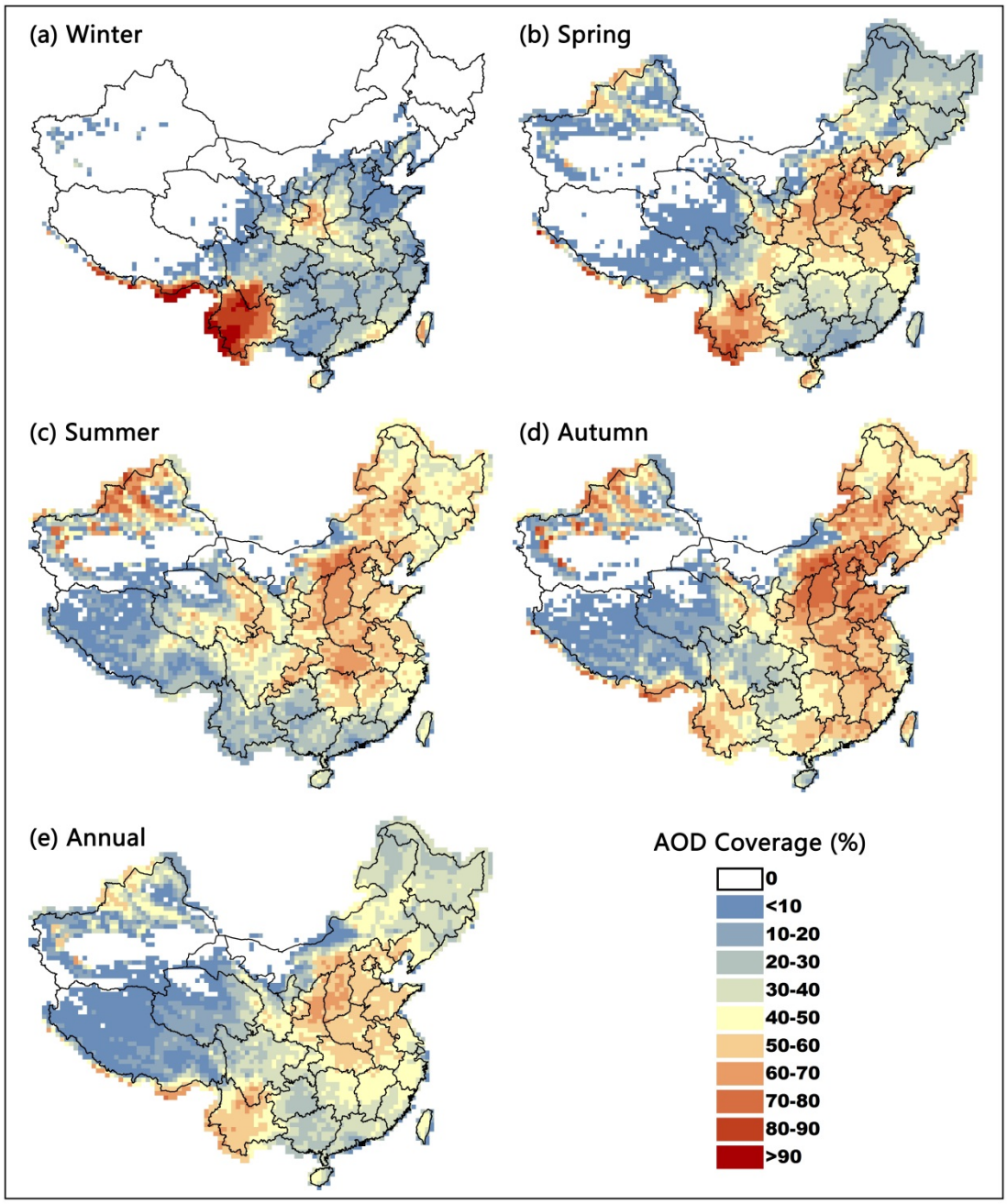

Figure S2. The spatial distribution of percent coverage of MODIS AOD.

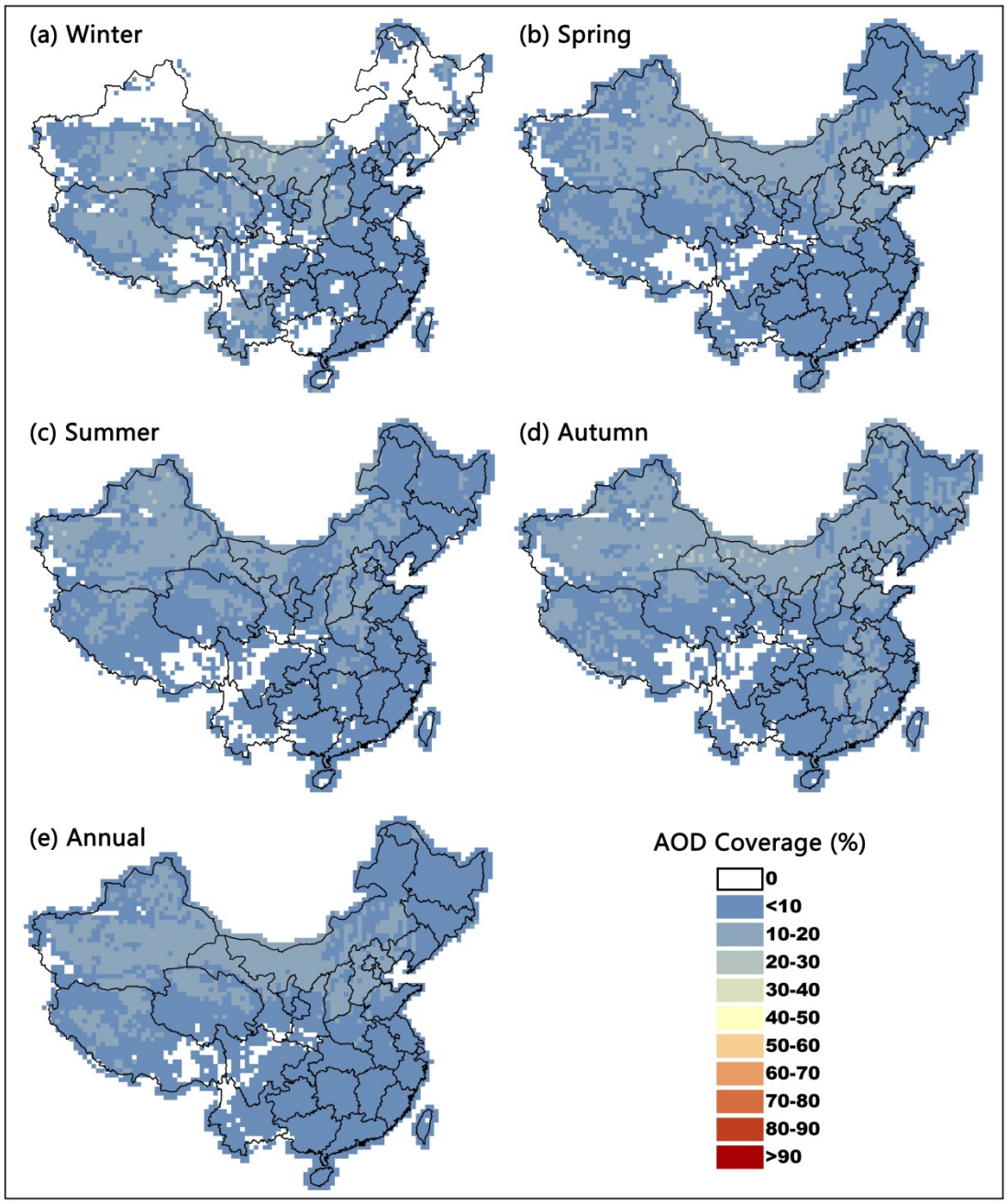

Figure S3. The spatial distribution of percent coverage of MISR AOD.

Text S3: Selection of meteorological and land use parameters.

First, we selected meteorological and land use parameters based on previous studies. Previous studies showed that meteorological parameters (e.g., boundary level height, temperature, relative humidity, and wind speed) and land use information (e.g., elevation, population, road length, emission source, and forest cover) are powerful predictors for ground $PM_{2.5}$ concentrations[10-14]. Given the data availability, we selected planetary boundary layer height (PBLH), temperature, wind speed, humidity, elevation, population (POP), and normalized difference vegetation index (NDVI) as the covariates in our GWR model. Elevation data were collected from Global Multi-resolution Terrain Elevation Data 2010 (GMTED2010) 30-arc-second product[15]. The meteorological data, population, and NDVI were collected from GEOS-FP, NEO, and LandScan, which are described in "MATERIALS AND METHODS" section, respectively.

We first evaluated potentially correlated parameters (i.e., temperature at 2 m above displacement height (T2M) vs. boundary-layer average temperature (T_PBLH), wind speed at 10 m above displacement height (WS) vs. boundary-layer average wind speed (WS_PBLH), elevation vs. surface pressure (PS)). These parameters are highly correlated ($R^2 > 0.9$). The results show that T2M, WS, and PS have better performance than other ones. Thus we selected PBLH, T2M, WS, RH_PBLH, PS, POP, and NDVI in our model. Our preliminary evaluation shows that those parameters are all statistically significant predictors.

We then compared the model performance of different combinations of AOD, meteorology, and land use parameters as predictors. Such comparison has been applied in a previous study [16]. Compared to the AOD-only model, despite a slight over-fitting in the "AOD plus LU" and "AOD plus

MET" model, the overall cross validation R^2, MPE, and RMSE are significantly improved (Table S2). Our results show that the meteorological and land use valuables included in our full model are powerful predictors for $PM_{2.5}$ in China.

Table S2 Results of model performance of different combinations of AOD, meteorology (MET), and land use (LU) parameters as predictors.

model	Model fitting			Model cross validation		
	R^2	MPE	RMSE	R^2	MPE	RMSE
Full	0.71	19.04	29.58	0.64	21.25	32.98
AOD-only	0.54	24.30	37.40	0.52	24.90	38.34
AOD plus LU	0.59	23.41	35.95	0.55	24.20	36.75
AOD plus MET	0.68	20.54	31.40	0.60	22.31	34.25
MET plus LU (non-AOD)	0.66	21.47	32.42	0.58	23.68	35.67

MPE: mean prediction error ($\mu g/m^3$). RMSE: root mean squared prediction error ($\mu g/m^3$).

Text S4: The selection of bandwidth

Studies have shown that the selection of bandwidth can greatly influence the performance of the Geographically Weighted Regression (GWR) model [17-19]. The bandwidth can be fixed or adaptive. Adaptive bandwidth is the optimal bandwidth selected by the Cross Validation (CV) method or Akaike's Information Criterion (AIC) [20, 21]. In this study, we examined model performance when using adaptive bandwidths selected by CV and AIC. Compared to a fixed bandwidth, our results show that adaptive bandwidths greatly increase over-fitting in the GWR models. For example, when the CV method is applied for adaptive bandwidth selection, the model fitting R^2 for the full model is 0.79. However, the model cross-validation R^2 decreases to 0.59. The root mean squared prediction error (RMSE) is 20.32 μg/m^3 for the model fitting. And the model cross-validation RMSE increases to 29.30 μg/m^3. Using AIC to obtain bandwidth for the full model also gives similar results. For these reasons, we selected a fixed bandwidth for our models.

Due to the uneven spatial distribution of ground $PM_{2.5}$ monitoring sites, the matched data records in Tibet and Xinjiang are important for modeling. We selected a fixed bandwidth of 800km. The distances between the $PM_{2.5}$ monitoring sites from both Tibet and Xinjiang to the border of the Tibetan Plateau are approximately 800 km. By using a fixed bandwidth of 800km, we can decrease the impact of Taklamakan Desert on the local relationship of Tibet and the impact of Tibetan Plateau on the local relationship of Xinjiang.

Text S5: Using Kriging to fill the AOD gaps.

As shown in Figure S1, AOD coverage in Western China (including Xinjiang and Tibet Autonomous Regions, and Qinghai Province) are relatively low, especially in winter. The density of ground $PM_{2.5}$ monitoring sites of this region is also relatively low. Thus, for many days, there are no matched data records in Xinjiang, Tibet, or Qinghai for GWR modeling. For example, Tibet has the following number of matched data records for GWR modeling: 1 day in winter, 11 days in spring, 25 days in summer, and 23 days in autumn. We cannot ascertain the local relationship between the dependent and independent variables for Tibet for the days missing matched data. To obtain the necessary matched data records for GWR modeling, we used the Ordinary Kriging method to interpolate AOD values in the grid cells that had ground-measured $PM_{2.5}$, but lacked AOD values. To make sure we only filled the missing AOD values that are spatially correlated with satellite-retrieved AOD values, we first obtained the range values by variogram analysis [22] for each day. We then created buffer zones for the grid cells that lack AOD values using the range values. If there were five or more grid cells with satellite-derived AOD values in the buffer zones, we obtained the interpolated AOD values of those AOD-missed grid cells.

To conduct the 10-fold cross-validation, at least 10 data points for GWR modeling are needed for each day. A previous study showed that model prediction becomes relatively stable when the number of matched data points is greater than 10 [12]. In this study, all days meet this condition after applying the Kriging method to fill the missing AOD values.

Here, we present the prediction maps using the model without interpolated the AOD values (Figure S4). Figure S4 shows the predicted concentrations in Tibet are relatively high, especially in winter

and spring; this does not agree with the ground monitoring results (Figure 4). We observed the true color images of MODIS from “NASA Worldview” (https://earthdata.nasa.gov/labs/worldview/) and found that the air in Tibet is clean where there are no clouds. Therefore, the predicted $PM_{2.5}$ values of Figure S4 are extremely overestimated in Tibet. There is more noise in model predictions for places like Xinjiang and Qinghai. However, the spatial patterns of predicted $PM_{2.5}$ are similar in areas with many of $PM_{2.5}$ ground monitoring sites, including North China Plain, Yangtze Delta, Taiwan, Southeast China, and Pearl River Delta, between Figure 4 and Figure S4. The results show that using the Kriging method to fill the AOD gaps can greatly improve the prediction accuracy in areas with a low density of $PM_{2.5}$ ground monitoring sites, without affecting the prediction accuracy in other areas.

We excluded days for which Tibet lacked ground $PM_{2.5}$ measurements in Figure 4. For those days, the matched data records could not be obtained, even though the Kriging method was applied to fill the AOD gaps. In total, 22 days of 344 were excluded, 12 of which were in winter and 10 were in the spring. When adding these days back to the prediction maps (Figure S5), we can see that $PM_{2.5}$ predictions in Tibet increase in the winter and spring. The matched data points in areas where ground monitoring sites are scarce are important for the prediction accuracy.

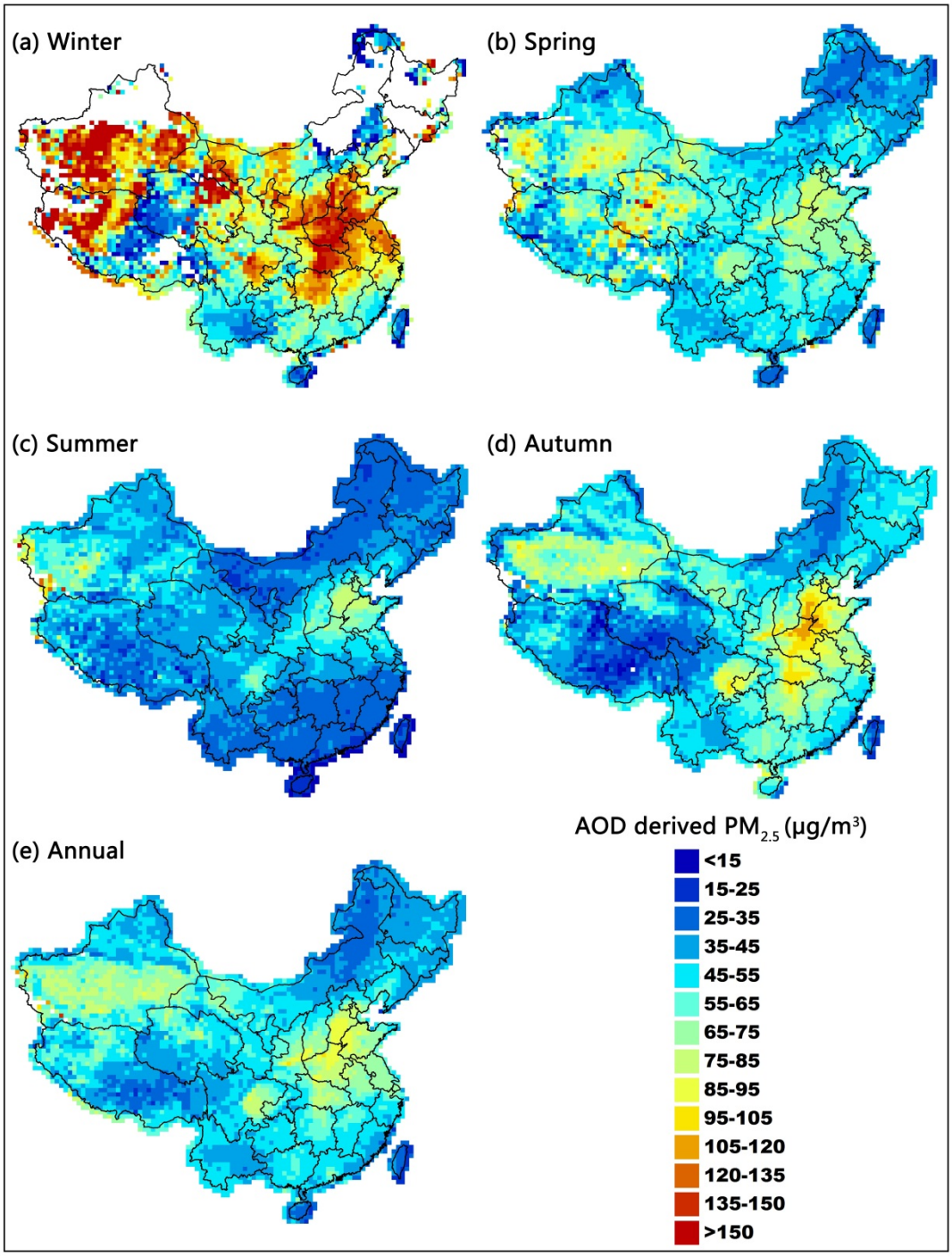

Figure S4. Predicted $PM_{2.5}$ concentrations by GWR without using Ordinary Kriging method to interpolate the missing AOD values in the grid cells with ground-measured $PM_{2.5}$ values.

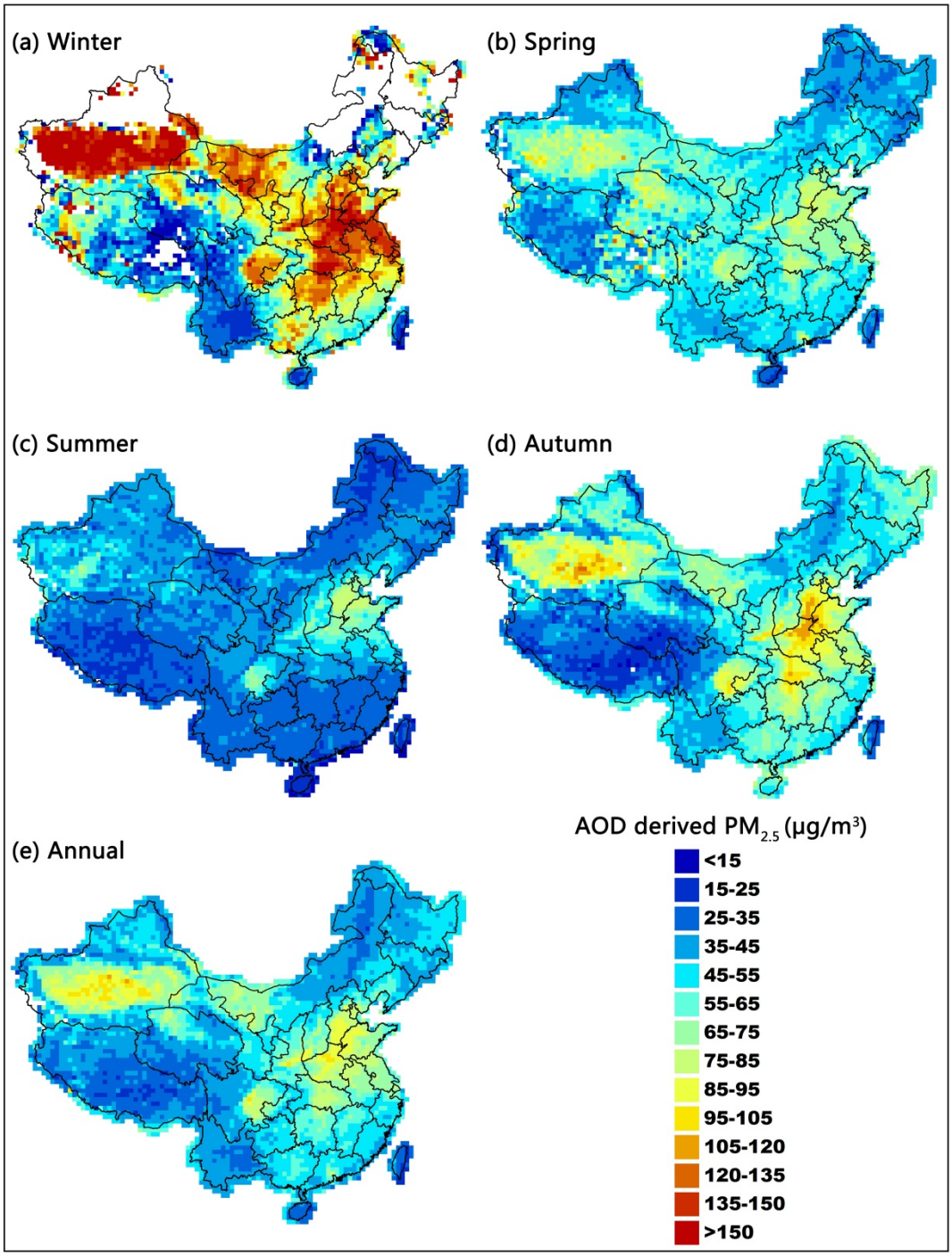

Figure S5. Predicted $PM_{2.5}$ concentrations by GWR using Ordinary Kriging method to interpolate the missing AOD values in the grid cells with ground-measured $PM_{2.5}$ values, but including the days when Tibet had no ground $PM_{2.5}$ measurements. In those days, the matched data records could not be obtained, even though the Kriging method was applied to fill the AOD gaps.

Other tables and figures:

Table S3 Descriptive statistics of the model datasets for each season

	Variable	Min	Max	Mean	Median	Std. Dev.
Winter	$PM_{2.5}$ (μg/m^3) [a]	2.75	795.00	101.65	76.50	83.89
(Dec-Feb, N=10 161)	AOD (Unitless) [b]	0.00	2.10	0.45	0.39	0.26
	PBLH (m) [c]	54.14	3469.02	785.99	764.16	419.80
	T2M (K) [d]	243.70	302.36	278.82	277.65	9.42
	WS (m/s) [e]	0.05	17.61	4.24	3.94	2.22
	RH_PBLH (%) [f]	7.17	99.27	67.71	72.47	20.65
	PS (hPa) [g]	585.74	1045.59	985.95	1014.54	71.05
	POP (People) [h]	1.79E+04	1.03E+07	2.01E+06	1.56E+06	1.78E+06
	NDVI (Unitless) [i]	-0.06	0.84	0.29	0.25	0.17
Spring	$PM_{2.5}$ (μg/m^3)	1.20	396.95	58.20	49.00	40.09
(Mar-May, N=14 742)	AOD (Unitless)	-0.01	3.99	0.59	0.53	0.36
	PBLH (m)	59.80	4021.07	1198.59	1151.26	561.02
	T2M (K)	259.60	313.29	291.73	293.02	7.85
	WS (m/s)	0.13	16.00	4.69	4.40	2.34
	RH_PBLH (%)	6.71	99.80	60.90	63.32	23.97
	PS (hPa)	587.73	1035.08	975.10	1002.84	68.12
	POP (People)	1.79E+04	1.03E+07	2.00E+06	1.53E+06	1.79E+06
	NDVI (Unitless)	-0.06	0.78	0.39	0.40	0.18
Summer	$PM_{2.5}$ (μg/m^3)	1.00	417.00	44.28	34.63	34.01
(Jun-Aug, N=16 293)	AOD (Unitless)	-0.04	3.83	0.45	0.36	0.37
	PBLH (m)	63.99	4005.77	1247.50	1241.21	467.30
	T2M (K)	281.64	313.14	301.97	302.51	4.28
	WS (m/s)	0.12	39.40	4.07	3.73	2.18
	RH_PBLH (%)	14.76	99.90	73.44	75.91	14.88
	PS (hPa)	593.49	1015.45	966.27	995.51	66.45
	POP (People)	1.79E+04	1.03E+07	1.98E+06	1.53E+06	1.76E+06
	NDVI (Unitless)	-0.04	0.83	0.57	0.60	0.16
Autumn	PM2.5 (μg/m^3)	3.00	753.00	66.49	53.40	49.52
(Sep-Nov, N=16 968)	AOD (Unitless)	-0.05	4.76	0.49	0.40	0.38
	PBLH (m)	58.27	3460.49	1132.62	1142.08	410.23
	T2M (K)	257.46	308.03	292.41	293.82	7.88
	WS (m/s)	0.12	25.06	4.26	3.81	2.40
	RH_PBLH (%)	9.80	99.90	62.41	64.87	20.80
	PS (hPa)	594.93	1032.60	978.41	1006.61	67.90
	POP (People)	1.79E+04	1.03E+07	1.94E+06	1.48E+06	1.72E+06
	NDVI (Unitless)	-0.02	0.83	0.44	0.43	0.17

[a] Daily ground-level PM2.5 concentrations. [b] Aerosol optical depth. [c] Planetary boundary layer height above surface. [d] Temperature at 2m above displacement height. [e] Wind speed at 10m above displacement height. [f] average relative humidity in PBLH layer. [g] Surface pressure. [h] Population. [i] Standard normalized difference vegetation index.

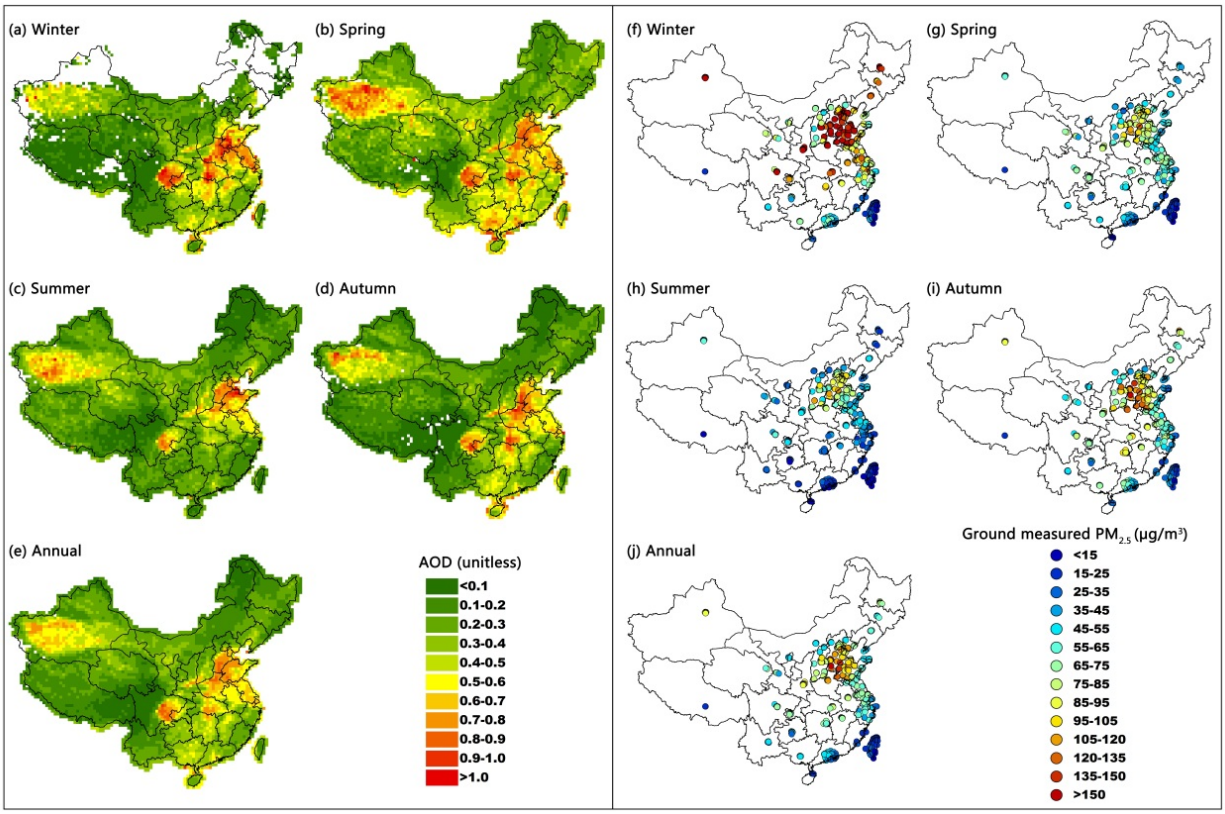

Figure S6. Spatial distributions of seasonal and annual mean fused AOD values and ground $PM_{2.5}$ measurements from all available days.

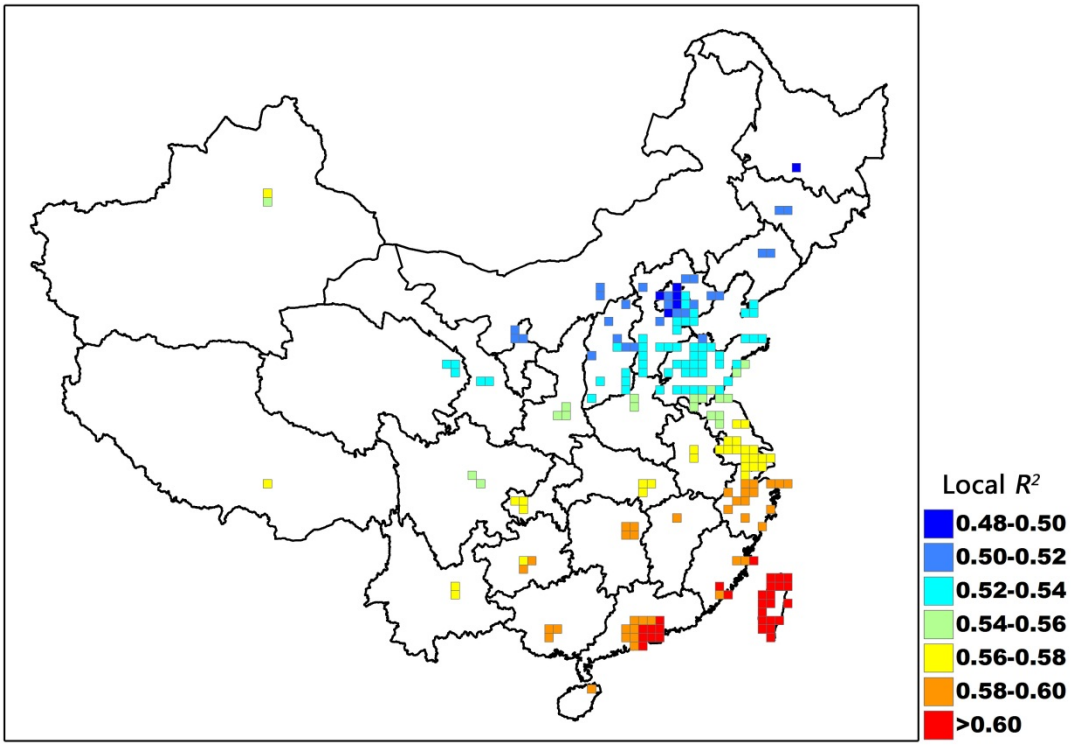

Figure S7. Spatial distributions of the grid cell mean local R^2 of the full model.

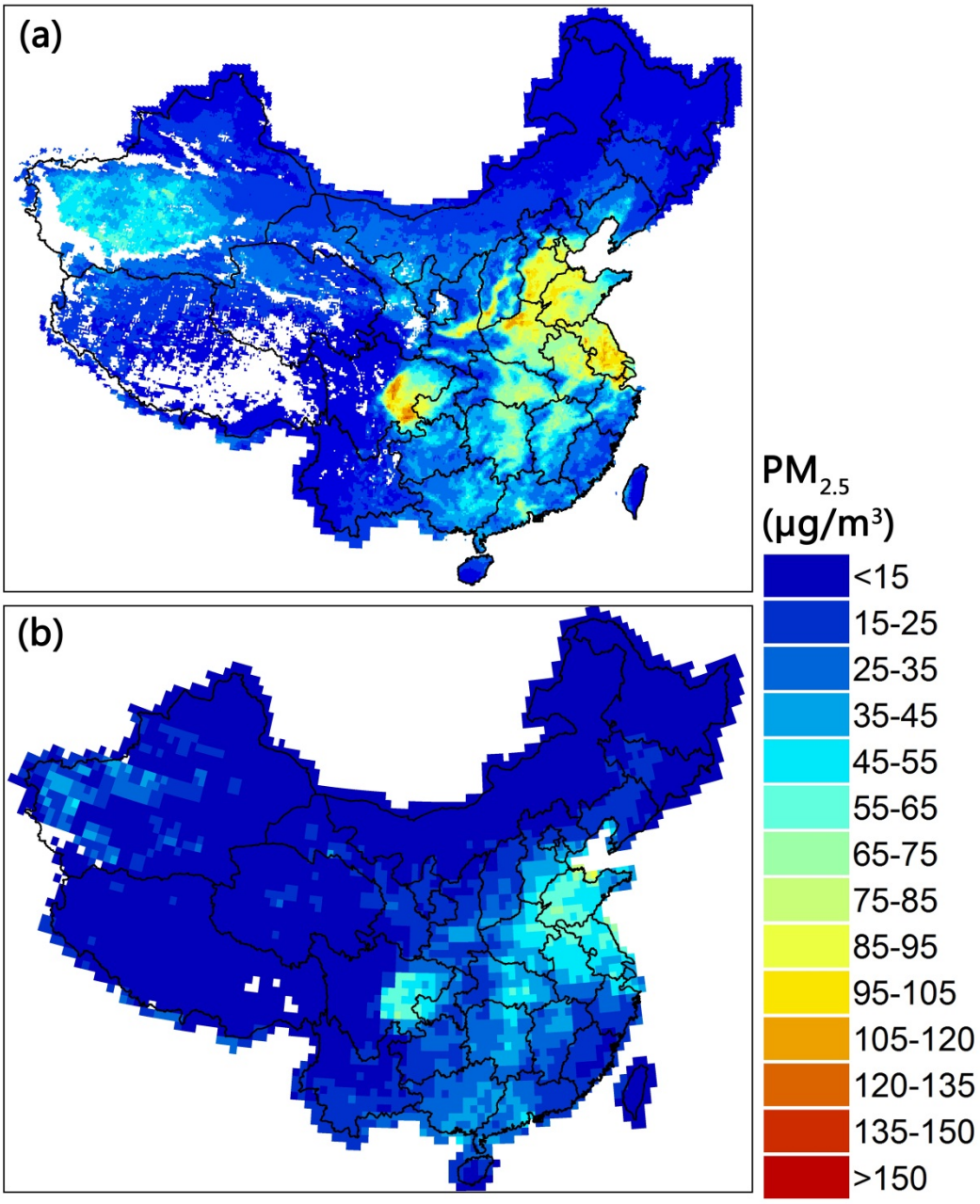

Figure S8. AOD-derived $PM_{2.5}$ maps from previous studies, which are re-plotted using the same color scale as Figure 4. (a) Mean estimated $PM_{2.5}$ of 2001-2006, from the study of van Donkelaar et al. [23]. (b) Mean estimated $PM_{2.5}$ of 2010, from the Center for International Earth Science Information Network (CIESIN) at Columbia University (http://sedac.ciesin.columbia.edu/data/set/sdei-global-annual-avg-pm2-5-2001-2010) [24]

References:

(1) Cheng, T.; Chen, H.; Gu, X.; Yu, T.; Guo, J.; Guo, H., The inter-comparison of MODIS, MISR and GOCART aerosol products against AERONET data over China. *J. Quant. Spectrosc. Radiat. Transf.* **2012**.

(2) Li, Z.; Niu, F.; Lee, K. H.; Xin, J.; Hao, W. M.; Nordgren, B.; Wang, Y.; Wang, P., Validation and understanding of Moderate Resolution Imaging Spectroradiometer aerosol products (C5) using ground‐based measurements from the handheld Sun photometer network in China. *J. Geophys. Res. Atmos.* **2007,** *112* (D22).

(3) Mi, W.; Li, Z.; Xia, X.; Holben, B.; Levy, R.; Zhao, F.; Chen, H.; Cribb, M., Evaluation of the moderate resolution imaging spectroradiometer aerosol products at two aerosol robotic network stations in China. *J. Geophys. Res. Atmos.* **2007,** *112* (D22), D22S08.

(4) Levy, R.; Remer, L.; Tanré, D.; Mattoo, S.; Kaufman, Y., Algorithm for remote sensing of tropospheric aerosol over dark targets from MODIS: Collections 005 and 051: Revision 2. *MODIS Algorithm Theoretical Basis Document for the MOD04_L2 Product* **2009**.

(5) Martonchik, J. V.; Kahn, R. A.; Diner, D. J., Retrieval of aerosol properties over land using MISR observations. In *Satellite Aerosol Remote Sensing Over Land*, Springer: 2009; pp 267-293.

(6) Hsu, N. C.; Tsay, S.-C.; King, M. D.; Herman, J. R., Aerosol properties over bright-reflecting source regions. *IEEE Trans. Geosci. Remote Sensing* **2004,** *42* (3), 557-569.

(7) Xie, Y.; Zhang, Y.; Xiong, X.; Qu, J. J.; Che, H., Validation of MODIS aerosol optical depth product over China using CARSNET measurements. *Atmospheric Environment* **2011,** *45* (33), 5970-5978.

(8) Levy, R. C.; Mattoo, S.; Munchak, L. A.; Remer, L. A.; Sayer, A. M.; Hsu, N. C., The Collection 6 MODIS aerosol products over land and ocean. *Atmos. Meas. Tech. Discuss.* **2013,** *6* (1), 159-259.

(9) Sayer, A. M.; Hsu, N. C.; Bettenhausen, C.; Jeong, M. J., Validation and uncertainty estimates for MODIS Collection 6 “Deep Blue” aerosol data. *j. Geophys. Res. Atmos.* **2013,** *118* (14), 7864-7872.

(10) Liu, Y.; Sarnat, J. A.; Kilaru, V.; Jacob, D. J.; Koutrakis, P., Estimating ground-level $PM_{2.5}$ in the eastern United States using satellite remote sensing. *Environ. Sci. Technol.* **2005,** *39* (9), 3269-3278.

(11) Liu, Y.; Paciorek, C. J.; Koutrakis, P., Estimating regional spatial and temporal variability of $PM_{2.5}$ concentrations using satellite data, meteorology, and land use information. *Environ. Health Perspect.* **2009,** *117* (6), 886-892.

(12) Hu, X.; Waller, L. A.; Al-Hamdan, M. Z.; Crosson, W. L.; Estes Jr, M. G.; Estes, S. M.; Quattrochi, D. A.; Sarnat, J. A.; Liu, Y., Estimating ground-level $PM_{2.5}$ concentrations in the southeastern US using geographically weighted regression. *Environ. Res.* **2013,** *121*, 1-10.

(13) Kloog, I.; Nordio, F.; Coull, B. A.; Schwartz, J., Incorporating local land use regression and satellite aerosol optical depth in a hybrid model of spatiotemporal $PM_{2.5}$ exposures in the Mid-Atlantic states. *Environ. Sci. Technol.* **2012,** *46* (21), 11913-11921.

(14) Hu, X.; Waller, L. A.; Lyapustin, A.; Wang, Y.; Al-Hamdan, M. Z.; Crosson, W. L.; Estes Jr, M. G.; Estes, S. M.; Quattrochi, D. A.; Puttaswamy, S. J., Estimating ground-level $PM_{2.5}$

concentrations in the Southeastern United States using MAIAC AOD retrievals and a two-stage model. *Remote. Sens. Environ.* **2014,** *140*, 220-232.

(15) Danielson, J.; Gesch, D., Global multi-resolution terrain elevation data 2010 (GMTED2010). *US Geology Survey Open File Report* **2011,** *2011-1073*, 25pp.

(16) Chang, H. H.; Hu, X.; Liu, Y., Calibrating MODIS aerosol optical depth for predicting daily PM2. 5 concentrations via statistical downscaling. *J. Expo. Sci. Env. Epid.* **2013**, 1-7.

(17) Shi, H.; Laurent, E. J.; LeBouton, J.; Racevskis, L.; Hall, K. R.; Donovan, M.; Doepker, R. V.; Walters, M. B.; Lupi, F.; Liu, J., Local spatial modeling of white-tailed deer distribution. *Ecological Modelling* **2006,** *190* (1), 171-189.

(18) Lloyd, C.; Shuttleworth, I., Analysing commuting using local regression techniques: scale, sensitivity, and geographical patterning. *Environment and Planning A* **2005,** *37* (1), 81-103.

(19) Windle, M. J.; Rose, G. A.; Devillers, R.; Fortin, M.-J., Exploring spatial non-stationarity of fisheries survey data using geographically weighted regression (GWR): an example from the Northwest Atlantic. *ICES Journal of Marine Science: Journal du Conseil* **2010,** *67* (1), 145-154.

(20) Guo, L.; Ma, Z.; Zhang, L., Comparison of bandwidth selection in application of geographically weighted regression: a case study. *Canadian Journal of Forest Research* **2008,** *38* (9), 2526-2534.

(21) Fotheringham, A. S.; Brunsdon, C.; Charlton, M., *Geographically weighted regression*. Wiley New York: 2002.

(22) Cressie, N. A., *Statistics for Spatial Data, revised edition*. Wiley, New York: 1993.

(23) van Donkelaar, A.; Martin, R. V.; Brauer, M.; Kahn, R.; Levy, R.; Verduzco, C.; Villeneuve, P. J., Global estimates of ambient fine particulate matter concentrations from satellite-based aerosol optical depth: development and application. *Environ. Health Perspect.* **2010,** *118* (6), 847.

(24) BMI&CIESIN, (Battelle Memorial Institute & Center for International Earth Science Information Network - Columbia University), Global Annual Average $PM_{2.5}$ Grids from MODIS and MISR Aerosol Optical Depth (AOD). In NASA Socioeconomic Data and Applications Center (SEDAC): 2013.